IEEE Photonics Journal
An IEEE Photonics Society Publication

Open Access

All-Angle Quasi-Self-Collimation Effect in a Rod-Type Silicon Photonic Crystal

Volume 7, Number 1, February 2015

Ming Li
Wei Li
Haiyang Huang
Jing Wang
You Li
Aimin Wu
Zhen Sheng
Xi Wang
Shichang Zou
Fuwan Gan

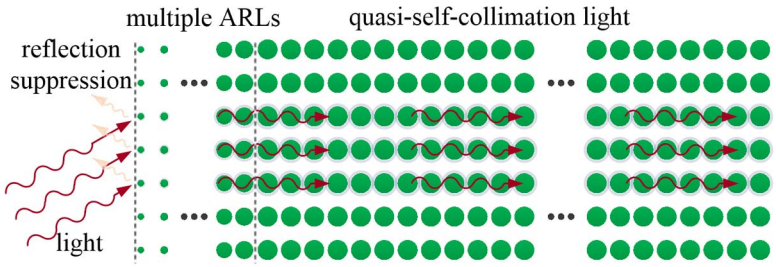

DOI: 10.1109/JPHOT.2015.2399433
1943-0655

All-Angle Quasi-Self-Collimation Effect in a Rod-Type Silicon Photonic Crystal

Ming Li,[1,2] Wei Li,[1] Haiyang Huang,[1,2] Jing Wang,[1,2] You Li,[1,2] Aimin Wu,[1] Zhen Sheng,[1] Xi Wang,[1] Shichang Zou,[1] and Fuwan Gan[1]

[1]State Key Laboratory of Functional Materials for Informatics, Shanghai Institute of Microsystem and Information Technology, Shanghai 200050, China.
[2]University of Chinese Academy of Science, Beijing 100049, China.

DOI: 10.1109/JPHOT.2015.2399433

Manuscript received December 24, 2014; revised January 27, 2015; accepted January 30, 2015. Date of publication February 11, 2015; date of current version February 18, 2015. This work was supported in part by the National Natural Science Foundation of China under Grant 61475180, Grant 61107031, Grant 11204340, and Grant 61275112, by the National High Technology Research and Development Program of China under Grant 2012AA012202, and by the Science and Technology Commission of Shanghai Municipality under Grant 14JC1407600. Corresponding authors: W. Li and F. Gan (e-mail: waylee@mail.sim.ac.cn; fuwan@mail.sim.ac.cn).

Abstract: By changing the symmetry of a photonic crystal (PC) with a rectangular lattice to straighten one of the isofrequency contours, the PC shows an all-angle quasi-self-collimation (quasi-SC) effect. To investigate the straightness of the isofrequency contour and the quasi-SC effect, we propose a straightness factor L based on the method of least squares. With $L \leq L_0$ ($L_0 = 0.01$ is the critical value), the isofrequency contour is sufficiently straight to induce the quasi-SC effect with the beam quasi-collimating in the structure. Furthermore, the efficiency of light coupling to the quasi-SC PC is studied and can be greatly improved by applying a carefully designed antireflection structure. This quasi-SC effect of the PC and the coupling structure may see applications in novel optical devices and photonic circuits.

Index Terms: Coupling efficiency, photonic crystals, quasi-self-collimation, antireflection layer.

1. Introduction

Over the past two decades, photonic crystals (PCs) have attracted much attention due to their potential application in the miniaturization and integration of optical devices [1]. They exhibit a variety of new physical phenomena, including a photonic bandgap (PBG) [2], the ability to act as a superprism [3], negative refraction [4], and self-collimation (SC)[5]. In an SC PC, the light beams propagate without diffraction, since their propagation directions are forced to be parallel to the group velocity, i.e., $\boldsymbol{V}_g = \nabla_k \omega(\boldsymbol{k})$, where ω is the optical frequency for a given wave vector $\boldsymbol{k}$. Therefore, the SC effect can be attributed to the flat part of the equi-frequency contours (EFCs) [6], [7]. The SC effect can be used to design a variety of novel SC-based photonic devices, such as channel-less waveguides [8], or devices for diffraction inhibition [9] and subwavelength focusing or imaging [10].

However, there are still a few issues that need to be addressed. For instance, the SC effect might be limited by the light incident angle, making it difficult for super-integrated devices based on the SC phenomenon. In this paper, we will present a model for an all-angle quasi-SC PC,

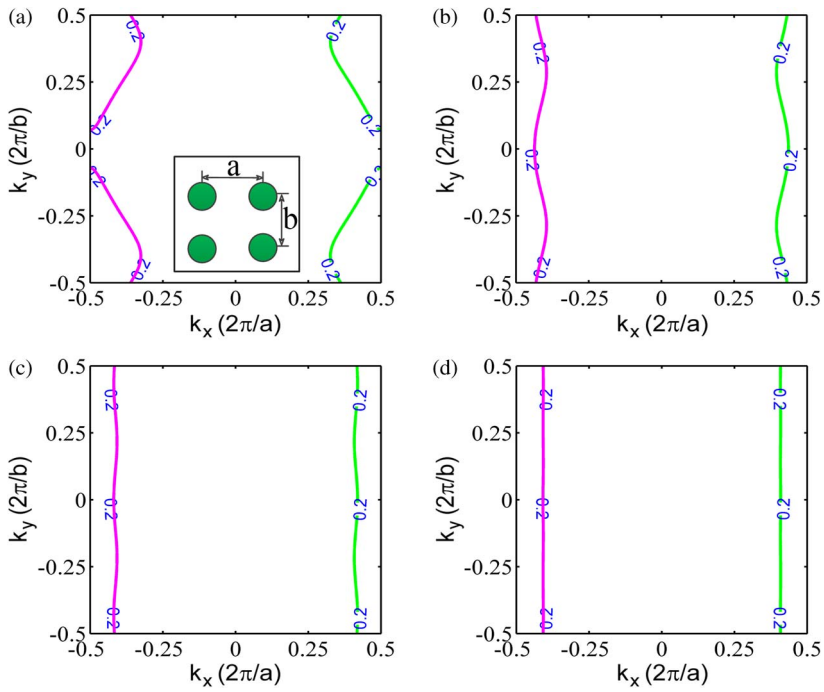

Fig. 1. EFCs for the normalized frequency $f = 0.2c/a$, fixed a, $r = 0.3a$, and different lattice length–breadth ratios β. (a) $\beta = 1.25$, (b) $\beta = 1.75$, (c) $\beta = 2.3$, and (d) $\beta = 3.5$. The inset image in (a) is the schematic illustration of the 2-D PC.

and lower the reflections for our quasi-SC PC by utilizing the destructive interference-based method.

2. Model

For this study, we consider a 2-D rod-type silicon PC with a rectangular lattice in the air, as shown on the inset image in Fig. 1(a). The length and breadth of the rectangular lattice are denoted by b and a, respectively, and the radius of the rod is $r = 0.3a$. The silicon rods are assumed to be lossless and nondispersive near the telecom frequency and exhibit a refractive index of 3.5. Utilizing the plane-wave expansion method, the EFCs are then calculated. For simplicity, throughout this paper, only one single frequency $f = 0.2c/a$ is considered for the transverse electric (TE) modes. This frequency is located in the first photonic band, and the corresponding isofrequency contour plot is shown in Fig. 1.

3. Results and Discussion

3.1. Straightness of the EFCs and Collimation Ability of the Beams

As shown in Fig. 1(a)–(d), by changing the symmetry of the PC, i.e., by increasing the length-breadth ratio $\beta = b/a$ of the rectangular lattice, an all-angle self-collimation effect can be eventually obtained for the PC. The all-angle effect is indicated by the straightness of the EFC which is plotted over the whole Brillouin zone in Fig. 1(d). As β increases, the light beams can reduce the beam divergence, resulting in a self-collimating propagation along the ΓX direction. Therefore, in order to improve the collimation ability, a higher straightness of the EFCs must be obtained. As illustrated by Fig. 1, the straightness quality of the EFCs depends on β.

To investigate the correlation between length-breadth ratio β and EFC straightness, we use the method of least squares [11] to quantify the EFC straightness, as shown in Fig. 1. According to the method of least squares, considering a quasi-straight EFC whose curve can be

represented by a function $Y = F(X)$ (Y and X representing the dimensionless $k_y/(2\pi/b)$ and $k_x/(2\pi/a)$ respectively), we assume that a straight line with the equation

$$\overline{Y} = AX + B \tag{1}$$

can be used to fit the quasi-straight EFC, where A and B are undetermined coefficients. In order to obtain A and B, we define $\varepsilon = \sum_{i=1}^{n}[Y_i - (AX_i + B)]^2$, where i is the number of sampling points, then, by utilizing the minimum condition, i.e., $\partial\varepsilon/\partial A = 0$, $\partial\varepsilon/\partial B = 0$, we obtain

$$A\sum X_i^2 + B\sum X_i = \sum X_i Y_i \tag{2}$$

and

$$A\sum X_i + nB = \sum Y_i \tag{3}$$

From (2) and (3), A and B can be calculated as follows:

$$A = \frac{n\sum X_i Y_i - \sum X_i \sum Y_i}{n\sum X_i^2 - (\sum X_i)^2}, \qquad B = \frac{\sum Y_i \sum X_i^2 - \sum X_i \sum X_i Y_i}{n\sum X_i^2 - (\sum X_i)^2}. \tag{4}$$

Finally, we can quantify the straightness quality of the EFCs via the straightness factor

$$L = \Delta L_{max} - \Delta L_{min} \tag{5}$$

where $\Delta L_{max} = [Y - \overline{Y}]_{max} = [Y - AX - B]_{max}$, and $\Delta L_{min} = [Y - \overline{Y}]_{min} = [Y - AX - B]_{min}$ are the maximum and the minimum convexities, respectively.

Physically, the straightness factor L as defined by (5) can be used to describe the averaged deviation angle of the propagation direction of a quasi-collimated light beam. For a quasi-collimated light beam, the beam width will become broader when the beam is propagating through the quasi-SC PC, with the waist of beam given by $W(D) \approx W_0 + L(\lambda D/\pi W_0)$ where λ is the wavelength in the air, W_0 and D (we assume $D \gg \lambda$, $D \gg W_0$) represent the initial waist and propagation distance of the beam, respectively. A smaller L corresponds to a straighter EFC and better self-collimation behavior. Only for $L = 0$ a perfectly straight EFC is obtained that corresponds to the strict self-collimation phenomenon without beam divergence, i.e., $W(D) = W_0$ for any D.

For most practical applications, the condition $L = 0$ is too strict. A sufficiently small L is usually acceptable. We suggest $L_0 = 0.01$ as the critical value for the straightness factor (corresponding to the pink dash line in Fig. 2). In this case, the quasi-collimated beam does hardly show any diffraction if $L \leq L_0$, e.g., with respect to a typical Gaussian beam with an initial waist $W_0 = 10\lambda$, the beam broadening is smaller than 1% as the beam propagates over a distance of 100λ. We suggest that such a quasi-collimated beam is sufficient for most practical applications with the self-collimation phenomenon.

Using (5), the straightness factor L of the EFCs at a single frequency can be calculated. The relation between the EFCs' straightness factor and the rectangular lattice structure is shown in Fig. 2. Apparently, the straightness factor L decreases as β increases. This result is in good agreement with the results presented in Fig. 1. In Fig. 1(a)–(d), the corresponding straightness factors are $L = 0.1743$, $L = 0.041$, $L = 0.01$ and $L = 8.09 \times 10^{-4}$ respectively. For the normalized frequency $f = 0.2c/a$, the condition $L = L_0$ corresponds to $\beta = 2.3$ with the corresponding EFC shown in Fig. 1(c). In order to provide additional information on the available operational frequencies of the quasi-SC effect, L as a function of β at other 4 frequencies is also shown in Fig. 2, from which we can see they are very similar to that of $f = 0.2c/a$. Also, by increasing β, the bandwidth of the quasi-SC effect becomes broader and broader since more and more EFCs have their straightness factor L smaller than L_0.

Fig. 2 suggests that, by increasing β, increasingly better SC can be achieved. For the case of $\beta \gg 1$, the system will become rows of rods that are isolated from each other, and consequently,

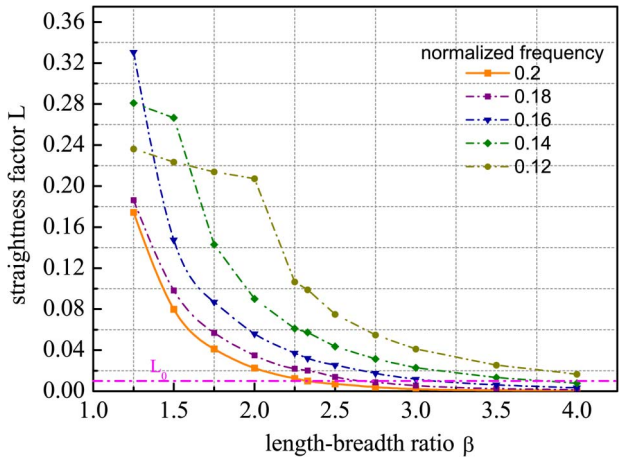

Fig. 2. Straightness factor L plotted as a function of the length–breadth ratio β of the rectangular lattice. The normalized frequencies are in unit of c/a.

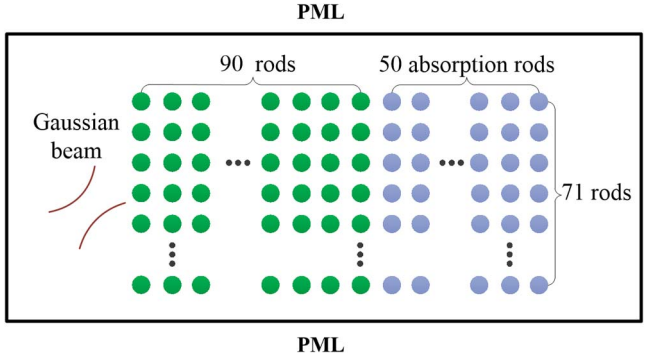

Fig. 3. FDTD calculation model.

in this case, we can just investigate only one single row of them. We find the SC effect is still valid in such a single row of rods. However, there are also many differences between the single row of them. We find the SC effect is still valid in such a single row of rods. However, there are also many differences between the single row and the PC with rectangular lattice. For simplicity, we constrain ourselves to only study the PC presented in Fig. 1 (with $\beta = 2.3$) at a single frequency $f = 0.2c/a$ in the following.

To show the all-angle quasi-collimation phenomenon of the PC at the frequency $f = 0.2c/a$, with $\beta = 2.3$, $a = 0.4$ μm, and $r = 0.3a$, a Gaussian beam with the beam width 2.3 μm (a little bit larger than one wavelength 2μm) is incident to the PC at different incident angles. The calculation model is shown in Fig. 3. A perfectly-matched-layer (PML) finite-differential-time-domain (FDTD) method [12], [13] with a grid size 20 nm is applied to calculate the electromagnetic field. To avoid the size-dependent Fabry-Perot effect, in the right end of the PC, a 50 $\times$ 71 rods array (the blue rods as shown in Fig. 3) is artificially set to be absorbed (a small imaginary part is added to the refractive index of rods, i.e., the index becomes 3.5 + 0.02i). The absorption rods array acts like a PML boundary condition for the PC. Therefore, this structure can be used to simulate an infinite-length PC. In Fig. 4 and the subsequent figures which show the field distribution, only the field in the non-absorption region is presented. Fig. 4(a)–(c) show the field distribution `when the Gaussian beam with different incident angle is propagating in the air (top panels) and the PC (lower panels). From Fig. 4, we can see the beam travels without beam divergence in the PC. In contrast, the beam diverges greatly in the air.

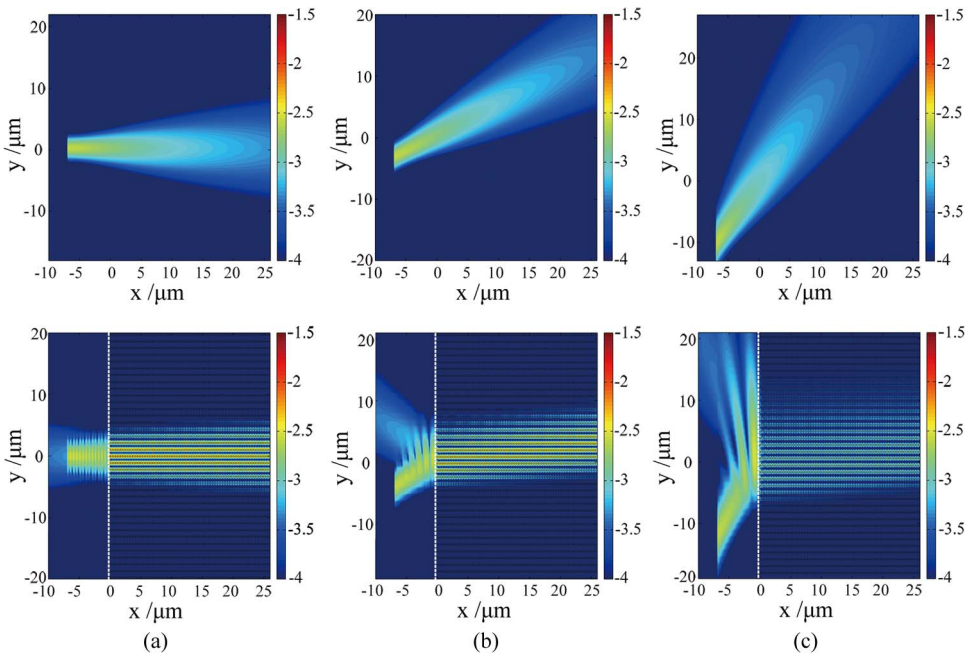

Fig. 4. Field distribution obtained for the illumination of a Gaussian beam into the air (top panel) and the PC (lower panel) with different incident angles θ. (a) $\theta = 0°$, (b) $\theta = 30°$, and (c) $\theta = 60°$. The white dashed line indicates the interface between the air and PC, and the field distribution is displayed using a logarithmic color map.

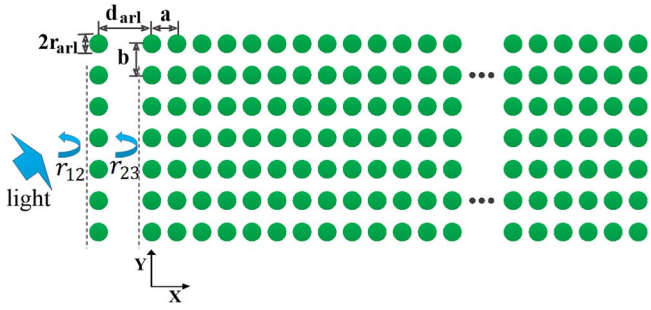

Fig. 5. Schematic illustration of the ARL placed in front of the quasi-SC PC. The variable ARL parameters are the distance d_{arl} and the radius r_{arl}.

3.2. Coupling Analysis

In this section, the efficiency of light coupling to the quasi-SC PC is studied. As shown in Fig. 4, large coupling losses (about 50%) occur due to the strong reflection. To improve the coupling efficiency, a destructive interference-based method is presented. As illustrated in Fig. 5, an antireflection layer (ARL) is applied in front of quasi-SC PC. The ARL also consists of an array of silicon rods with the lattice constant $b = 2.3a$, which is equal to the length of the quasi-SC PC's rectangular lattice. The radius of the silicon rods in the ARL is r_{arl}, and the distance between the ARL and the quasi-SC PC is d_{arl}. The parameters d_{arl} and r_{arl} should be well-designed to improve the coupling efficiency.

The coupling efficiency $\kappa = 1 - |r_{tot}|^2$ is directly determined by the total reflection coefficient r_{tot}, which can be written as

$$r_{tot} = \frac{r_{12} + r_{23}e^{i2\alpha}}{1 + r_{12}r_{23}e^{i2\alpha}} \tag{6}$$

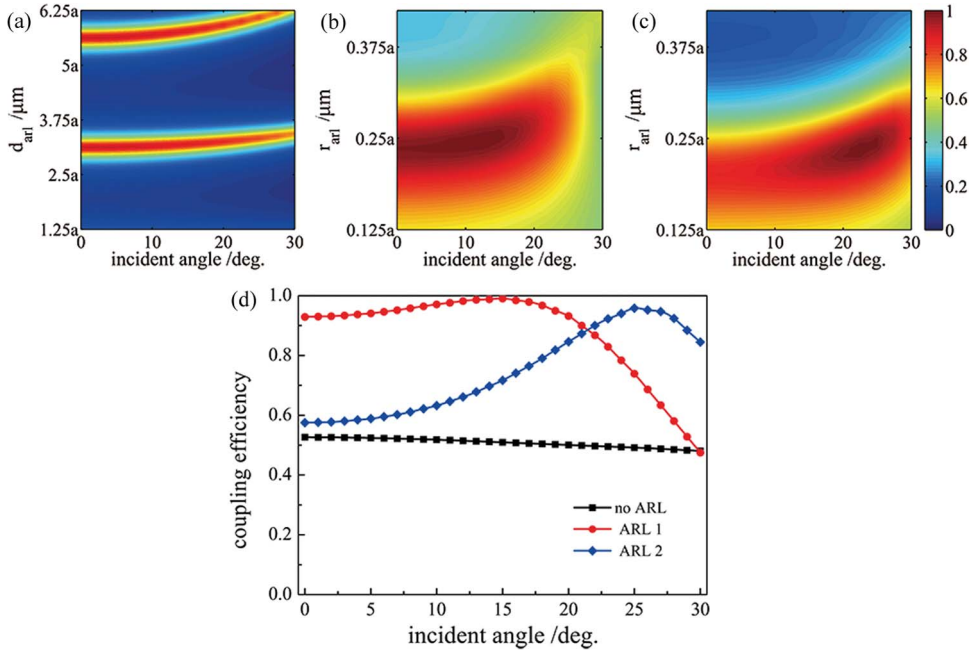

Fig. 6. (a) Coupling efficiency as a function of d_{arl} and the incident angle for r_{arl} fixed at 0.3a. (b) Coupling efficiency as a function of r_{arl} and an incident angle θ for an optimized $d_{arl} = 3.28a$. (c) Coupling efficiency as a function of r_{arl} and an incident angle θ for an optimized $d_{arl} = 3.44a$. (d) Coupling efficiency as a function of the incident angle without and with ARL. The structure parameters of ARL 1 and ARL 2 are $d_{arl} = 3.28a$, $r_{arl} = 0.26a$, and $d_{arl} = 3.44a$, $r_{arl} = 0.26a$, respectively.

where $\alpha = k_0 \cdot (d_{arl} - r - r_{arl})$ is the phase shift of the light beam as it crosses the ARL (k_0 denotes the wave vector in the air), r_{12} is the reflection coefficient of the ARL in the air, and r_{23} is the reflection coefficient of the semi-infinite quasi-SC PC when the light beam is hitting the PC surface from air. Both r_{12} and r_{23} can be calculated by applying the multiple scattering method [14].

Now, we try to find suitable r_{arl} and d_{arl} values in order to reduce the total reflection $|r_{tot}|^2$. First, the coupling efficiency for an initial value of r_{arl} with $r_{arl} = r$ is calculated, and the resulting color map is shown in Fig. 6(a). In this figure, the red region corresponds to a high coupling efficiency. As shown in Fig. 6(a), there are two regions that allow for a high coupling efficiency for a relatively wide range of incident angles. One can choose suitable d_{arl} according to Fig. 6(a), e.g., for a d_{arl} of approx. 3.28a for incident angle 0° to 20°, or 3.44a for incident angle 20° to 30°. Then, for the optimized d_{arl}, one can further improve the coupling efficiency by optimizing r_{arl}, as shown in Fig. 6(b) and Fig. 6(c). In Fig. 6(b) and Fig. 6(c), the values of d_{arl} are fixed to be 3.28a and 3.44a, respectively. The enhanced coupling efficiency versus incident angle is shown in Fig. 6(d). From Fig. 6(d), we can see by using the well-designed ARL, the coupling efficiency is greatly improved for a wide incident angle range.

To further improve the coupling efficiency, we provide graded multiple ARLs with the same lattice constant $(b = 2.3a)$ located in front of the photonic crystal at a distance a, as shown in Fig. 7(a). The graded multiple ARLs have 20 layers, and the radius of rods is slowly varying from the left to the right, i.e., for the ith layer, the radius of the rods is $r_{ARLS}(i) = i(r/20)$, where $i = 1, 2, \ldots, 20$. By using the multiple ARLs, the coupling efficiency is improved for nearly all incident angles, as shown in Fig. 7(b).

To validate the improvement of the coupling efficiency, we calculated the field distribution for a Gaussian beam at 4 incident angles launching at the PC with multiple ARLs, and the resulting field distributions are respectively shown in Fig. 8(a)–(d). For the multiple ARLs structure, the Gaussian beams almost perfectly couple into the PC with almost no reflection. Comparing Fig. 8 with Fig. 4, the reflection is suppressed by the multiple ARLs.

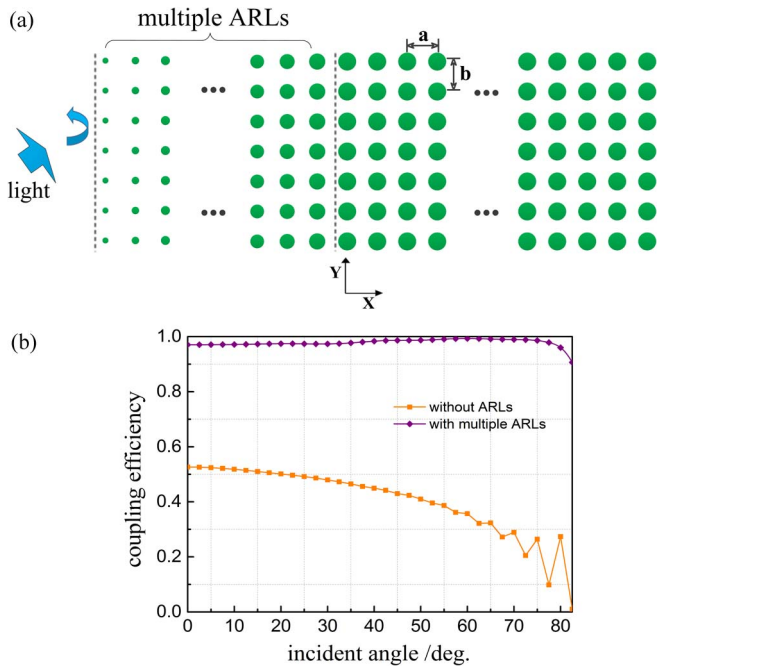

Fig. 7. (a) Schematic illustration of the multiple ARLs. (b) Coupling efficiency as a function of the incident angle without and with multiple ARLs.

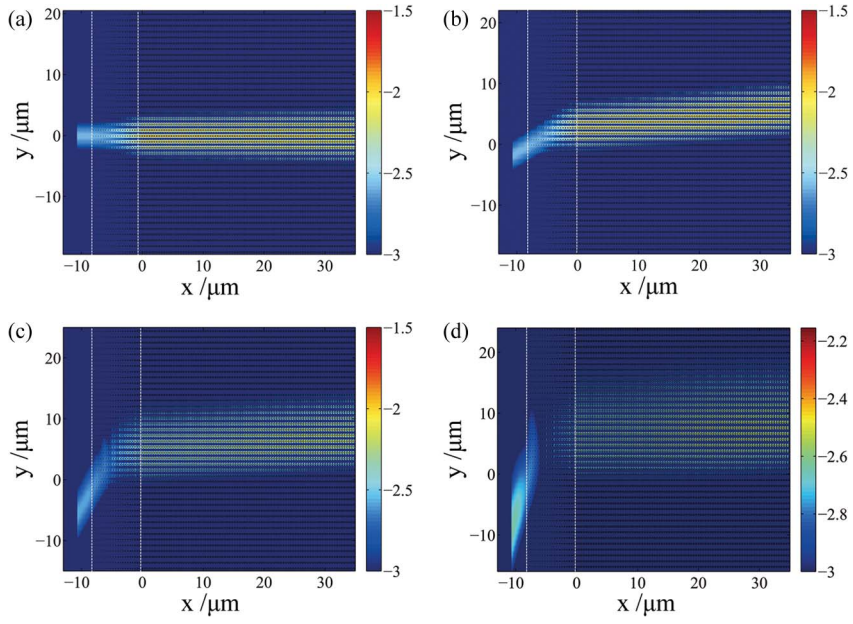

Fig. 8. Field distribution for a Gaussian beam launching at the PC with multiple ARLs at different incident angles θ. (a) $\theta = 0°$, (b) $\theta = 30\circ$, (c) $\theta = 60°$, and (d) $\theta = 75°$. The white dashed line indicates the interface, and the field distribution is displayed using a logarithmic color map.

4. Conclusion

In this paper, a quasi-self-collimation effect is obtained by changing the symmetry of a rectangular-lattice photonic crystal. The quasi-self-collimation effect is quantified by a straightness factor *L* that is based on the method of least squares. When the straightness factor *L* decreases, the photonic

crystal possesses a more powerful self-collimation effect. Besides, the efficiency of light coupling to the quasi-SC PC is investigated and is greatly improved by applying a carefully designed antireflection structure. This quasi-SC effect of the PC, as well as the coupling structure, may see applications in novel optical devices and photonic circuits.

References

[1] M. Qi *et al.*, "A three-dimensional optical photonic crystal with designed point defects," *Nature*, vol. 429, no. 6991, pp. 538–542, Jun. 2004. [Online]. Available: www.nature.com/articles/nature02575

[2] E. Yablonovitch, "Inhibited spontaneous emission in solid-state physics and electronics," *Phys. Rev. Lett.*, vol. 58, no. 20, pp. 2059–2062, Dec. 1987. [Online]. Available: http://journals.aps.org/prl/abstract/10.1103/PhysRevLett.58.2059

[3] W. Li, X. G. Zhang, X. L. Lin, and X. Y. Jiang, "Enhanced wavelength sensitivity of the self-collimation superprism effect in photonic crystals via slow light," *Opt. Lett.*, vol. 39, no. 15, pp. 4486–4489, Aug. 2014. [Online]. Available: http://www.opticsinfobase.org/ol/abstract.cfm?uri=ol-39-15-4486

[4] P. J. Yao, W. Li, S. L. Feng, and X. Y. Jiang, "The temporal coherence improvement of the two-dimensional negative-index slab image," *Opt. Exp.*, vol. 14, no. 25, pp. 12295–12301, Dec. 2006. [Online]. Available: http://www.opticsinfobase.org/oe/abstract.cfm?uri=oe-14-25-12295

[5] H. Li *et al.*, "Millimeter-scale and large-angle self-collimation in a photonic crystal composed of silicon nanorods," *IEEE Photon. J.*, vol. 5, no. 2, Apr. 2013, Art. ID. 2201306. [Online]. Available: http://ieeexplore.ieee.org/xpls/abs_all.jsp?arnumber=6504461

[6] R. S. Chu and T. Tamir, "Group velocity in space-time periodic media," *Electron. Lett.*, vol. 7, no. 14, pp. 410–412, Jul. 1971. [Online]. Available: http://digital-library.theiet.org/content/journals/10.1049/el_19710278

[7] T. Yamashita and C. J. Summers, "Evaluation of self-collimated beams in photonic crystals for optical interconnect," *IEEE J. Sel. Areas Commun.*, vol. 23, no. 7, pp. 1341–1347, Jul. 2005. [Online]. Available: http://ieeexplore.ieee.org/xpls/abs_all.jsp?arnumber=1461493

[8] H. Kosaka *et al.*, "Self-collimating phenomena in photonic crystals," *Appl. Phys. Lett.*, vol. 74, no. 9, pp. 1212–1214, Mar. 1999. [Online]. Available: http://scitation.aip.org/content/aip/journal/apl/74/9/10.1063/1.123502

[9] L. L. Zhang, Q. W. Zhan, J. Y. Zhang, and Y. P. Cui, "Diffraction inhibition in two-dimensional photonic crystals," *Opt. Lett.*, vol. 36, no. 5, pp. 651–653, Mar. 2011. [Online]. Available: http://www.opticsinfobase.org/ol/fulltext.cfm?uri=ol-36-5-651&id=210164

[10] C. Lv, W. Li, X. Y. Jiang, and J. C. Cao, "Far-field super-resolution imaging with a planar hyperbolic metamaterial lens," *Europhys. Lett.*, vol. 105, no. 2, Jan. 2014, Art. ID. 28003. [Online]. Available: http://iopscience.iop.org/0295-5075/105/2/28003

[11] H. Abdi, "The method of least squares," in *Encyclopedia of Research Design.* Thousand Oaks, CA, USA: Sage, 2007, pp. 705–708. [Online]. Available: http://www.utd.edu/~herve/Abdi-LeastSquares06-pretty.pdf

[12] W. Li, Z. Liu, X. Zhang, and X. Jiang, "Switchable hyperbolic metamaterials with magnetic control," *Appl. Phys. Lett.*, vol. 100, no. 16, Aug. 2012, Art. ID. 161108. [Online]. Available: http://scitation.aip.org/content/aip/journal/apl/100/16/10.1063/1.4705084

[13] A. Taflove and S. C. Hagness, *Computational Electrodynamics: The Finite-Difference Time-Domain Method*, 3th ed. Boston, MA, USA: Artech House, May 2005.

[14] H. Li *et al.*, "Optical total reflection and transmission with mode control in a dielectric subwavelength nanorod chain," *Chin. Phys. B*, vol. 22, no. 11, Nov. 2013, Art. ID. 117807. [Online]. Available: http://iopscience.iop.org/1674-1056/22/11/117807